

High-temperature tensile behavior of freestanding Au thin films

Gi-Dong Sim, Joost J. Vlassak*

School of Engineering and Applied Science, Harvard University, Cambridge, Massachusetts
02138, USA

Abstract

The mechanical behavior of freestanding thin sputter-deposited films of Au is studied at temperatures up to 340°C using tensile testing. Films tested at elevated temperatures exhibit a significant decrease in flow stress and stiffness. Furthermore the flow stress decreases with decreasing film thickness, contravening the usual notion that “smaller is stronger”. This behavior is attributed mainly to diffusion-facilitated grain boundary sliding.

Keywords: In situ tensile test, High-temperature deformation, Thin films, Grain boundary sliding, Creep

1. Introduction

The decreasing size of microelectronics devices has motivated a strong interest in the effects of length scales on the mechanical behavior of thin films of metal. As a result, metal thin films, which are key components in these devices, have been studied extensively. These investigations have demonstrated that the mechanical properties of thin films are generally very different from those of their bulk counterparts [1-11] and that they depend on whether the film is freestanding or supported by a substrate [12-15]. Understanding the mechanical behavior of metal thin films at elevated temperature is essential for the design of reliable devices, which often operate above room temperature. Several studies have been performed on the high-temperature behavior of films on substrates [2, 16-19], but studies on freestanding films have been limited to temperatures below 200°C [20-23] due to difficulties associated with sample handling, oxidation, and temperature uniformity in the sample. The few studies performed at higher temperatures focused on films that were several microns thick [24-26]. Thus, the high-temperature behavior of freestanding metal thin films is still relatively unexplored.

Recently, we developed a technique for the tensile testing of freestanding thin films in which samples were mounted on a micro-machined silicon frame with integrated heaters [27]. The samples were deformed in-situ inside a scanning electron microscope (SEM) by means of a custom-built test apparatus. Using this technique, the stress-strain curves of copper thin films were measured at temperatures up to 430°C. In this paper, the same technique is used to characterize the mechanical behavior of gold films as a function of temperature and strain rate. Gold was chosen as the material of interest due to its oxidation resistance and low electrical resistivity. The oxidation resistance makes gold an interesting material for studying the inherent mechanical behavior at elevated temperature without the added complication of a passivation

layer. Gold films are also increasingly used in a broad range of devices and sensors [24-26].

2. Materials and methods

2.1. Specimen preparation and material characterization

Silicon frames with integrated micro-heaters were fabricated using standard photolithography and silicon micromachining techniques (Figure 1). As part of the fabrication process of the test frames, Au films with thicknesses of 450 and 960 nm were deposited using a magnetron sputter deposition system (AJA International) with a base pressure of 1×10^{-7} Pa. The films were sputtered from a 50.8 mm Au target using a DC power of 200 W and the deposition proceeded in an atmosphere of 0.67 Pa of Ar. After deposition, all sample frames were annealed at 400°C for one hour in vacuum to stabilize the microstructure of the Au films during testing and to stabilize the tungsten heating elements of the integrated micro-heaters. Samples were fabricated with gauge widths of 100, 150, and 200 μm , and gauge lengths of 1232 ± 12 and 2425 ± 19 μm . While the widths of the samples were very precise, the gage lengths varied slightly depending on process conditions. Each 55×55 mm Si substrate contained 28 individual samples. A detailed account of the fabrication process can be found in Ref. [27].

The grain structure of the samples was characterized in a Zeiss Ultra55 field-emission scanning electron microscope (FE-SEM, Carl Zeiss Inc. Thornwood, NY) and a Zeiss NVision 40 Dual-Beam focused ion beam and scanning electron microscope (FIB/SEM). The crystallographic texture of the films was measured using electron backscatter diffraction (EBSD) inside the Zeiss Supra55 FE-SEM. Film thicknesses were measured using a profilometer (Veeco Dektak 6M).

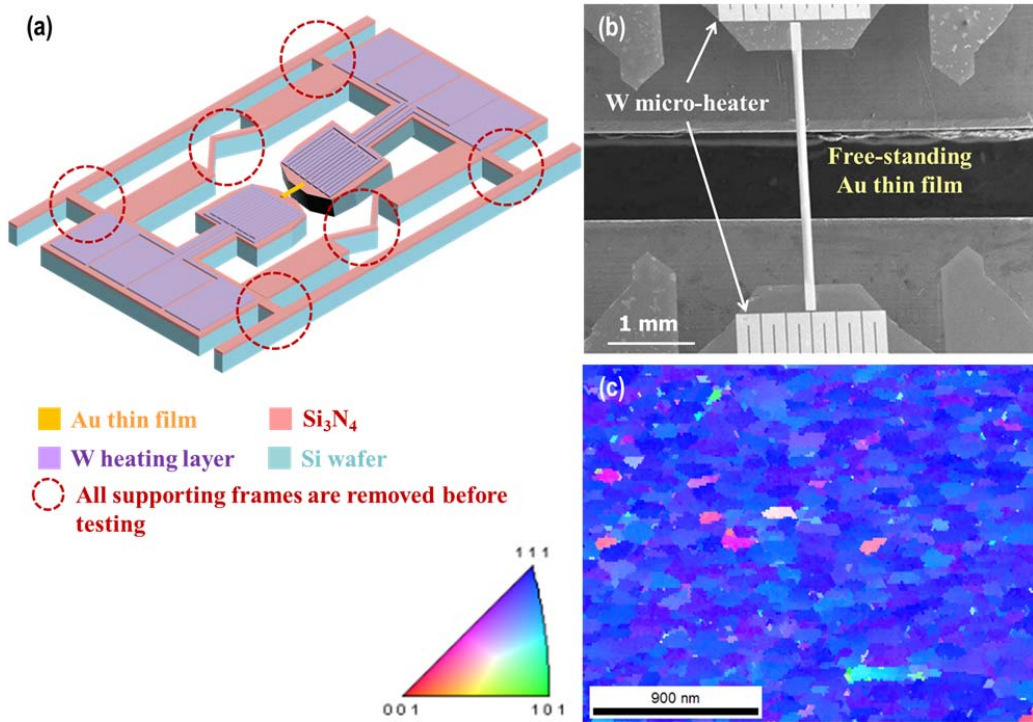


Figure 1. (a) Schematic image of the micro heater and sample. (b) SEM image of the fabricated freestanding Au thin film and (c) EBSD image showing the grain structure and the crystallographic texture of a 960 nm thick Au film.

2.2. Tensile testing at elevated temperatures

All tensile experiments were performed inside an SEM using a custom-designed tensile tester described in detail in reference [27]. This tensile tester has a total stroke of 250 μm , a displacement resolution of 10 nm, and a load resolution of 9.7 μN . The micro-machined sample frames have two sets of supports to facilitate sample handling (Figure 1). The outermost set provides protection while the sample is mounted in the tensile tester. Once mounted, the innermost supports protect the sample, while the outermost supports are removed. Finally the innermost supports are snapped by loading the sample in compression.

Tests were performed at different strain rates ranging from $2.0 \times 10^{-4} \text{s}^{-1}$ to $2.0 \times 10^{-5} \text{s}^{-1}$ and at temperatures up to 340°C. For measurements at elevated temperatures, the micro-heaters were turned on inside the SEM chamber by passing a current through the heating elements, while the resistance of the heating elements was measured in a four-point measurement setup. During the experiment, the temperature of the micro-heaters was determined from the resistance of the heating elements, which was calibrated to temperature using

$$T = T_0 + \frac{R_{MH} - R_{MH,0}}{\lambda R_{MH,0}}, \quad (1)$$

where λ is the temperature coefficient of resistance of the heating element, R_{MH} is the resistance of the heating element, T_0 is the ambient temperature, and $R_{MH,0}$ is the resistance at T_0 . The temperature coefficient of resistance λ was measured prior to the high-temperature experiment by placing the sample frame on a hot plate and by measuring the resistance of the micro-heater using a Keithley 2000 multimeter in a four-terminal setup, while increasing the temperature up to 180°C. The temperature coefficient of resistance λ was then determined from a linear least squares fit of the resistance data as a function of temperature. Finite element modeling in our

prior work [27] has demonstrated that this experimental setup results in a temperature distribution throughout the tensile sample with better than 99% uniformity, as long as the temperature is below 1200°C. Further specifications of the tensile tester and the micro-heaters can be found in Ref. [27].

3. Experiment results

3.1. Microstructure

Figure 1 (c) shows an EBSD image of the microstructure of a typical 960 nm Au film. The grain size was measured using the linear intercept method and was virtually independent of film thickness. EBSD images also provided the crystallographic texture of the films, which had a strong (1 1 1) fiber component for all films. A summary of the microstructure data is provided in Table I.

Table I.

Microstructure of the Au thin films

Thickness, h (nm)	Grain size, d (nm)	$f_{(111)}$ ^a (%)
450 ± 4	112 ± 14	96.4
960 ± 8	131 ± 14	91.5

^a Volume fraction of grains within 10° of (111) orientation

3.2. Experimental results

Figure 2(a) shows the stress-strain curves of the 450 nm Au films obtained for different temperatures at a strain rate of $2.0 \times 10^{-5} \text{ s}^{-1}$; Figure 2(b) shows the stress-strain curves of the 940 nm films for a range of temperatures and strain rates. Two features stand out: the slopes of the loading and unloading curves decrease dramatically with rising temperature, as does the flow stress. The loading slopes and flow stress are summarized in Table II.

The unloading curve has an initial slope of $71.3 \pm 3.1 \text{ GPa}$, but is otherwise quite nonlinear, indicative of anelastic behavior. Anelasticity in metals is typically attributed to dislocation bowing or grain boundary sliding [23]. Dislocation bowing can cause at most a 10% decrease of the modulus [28], making grain boundary sliding the more plausible explanation. The loading slopes of the stress-strain curves measured at elevated temperature (Table II) show significant reductions compared to the room temperature value, and this reduction is virtually independent of film thickness. A similar but much smaller effect is observed with decreasing strain rate.

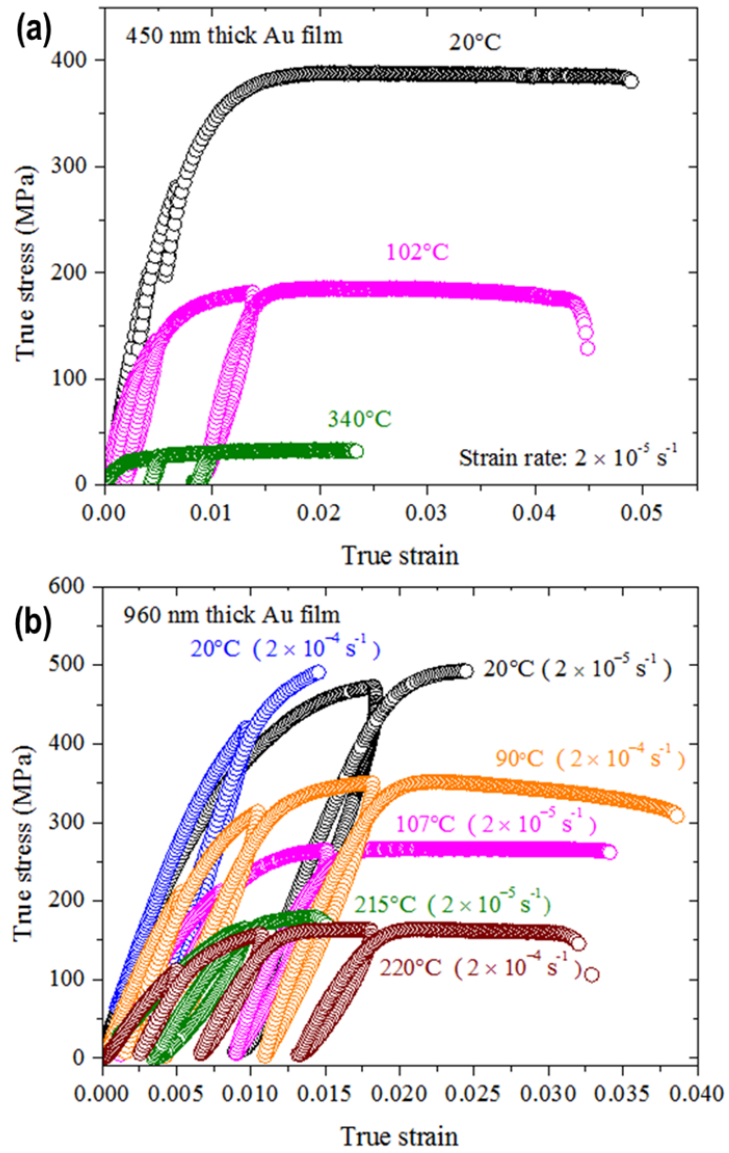


Figure 2. True stress-strain curve of (a) 450 nm and (b) 960 nm Au films showing both temperature and strain rate effects.

The effect of temperature on the flow stress of the films is even more dramatic, with reductions as large as an order of magnitude. Measurements performed at smaller strain rates also result in significantly lower flow stress, evidence of a strong strain-rate effect. Similar observations have been made at lower temperatures in prior studies on thin films of Au [21, 29-31] and other fcc materials, including Cu [32] and Ni [33]. Another interesting observation is that the flow stress of the 940 nm films is somewhat greater than that of the 450 nm films, and that this difference increases with increasing temperature, contravening the usual notion that smaller is stronger.

Figure 3 shows a series of SEM micrographs of the regions where the films fractured, taken at the conclusion of tensile tests performed at different temperatures and strain rates. Films tested above 200 °C show extensive grain boundary voiding, indicative of significant grain boundary diffusion during the deformation process, while films tested at lower temperatures show no such voiding.

Table II.

Summary of the experimental results

Thickness, h (nm)	Strain rate, $\dot{\epsilon}$ (s^{-1})	Temperature ($^{\circ}C$)	Loading slope (GPa)	Flow stress ^a (MPa)	Ashby Model (MPa)
450 ± 4	2.0×10^{-5}	20	63.3 ± 1.1	383 ± 4	6.5×10^4
		102	55.2 ± 1.6	181 ± 2	42
		340	32.1 ± 0.4	31 ± 1	1.3
960 ± 8	2.0×10^{-4}	20	61.8 ± 0.1	512 ± 5^b	1.0×10^6
		90	57.4 ± 1.7	346 ± 4	1.6×10^3
		220	36.2 ± 0.7	163 ± 2	2.4
	2.0×10^{-5}	20	60.3 ± 0.7	470 ± 5	1.0×10^5
		107	50 ± 3.4	265 ± 3	47
		215	32.5 ± 0.1	180 ± 2	1.3

^a The flow stress is defined as the flow stress at 1% permanent strain for all films^b Value estimated by shifting the corresponding $2 \times 10^{-5} s^{-1}$ stress-strain curve to coincide with the $2.0 \times 10^{-4} s^{-1}$ curve

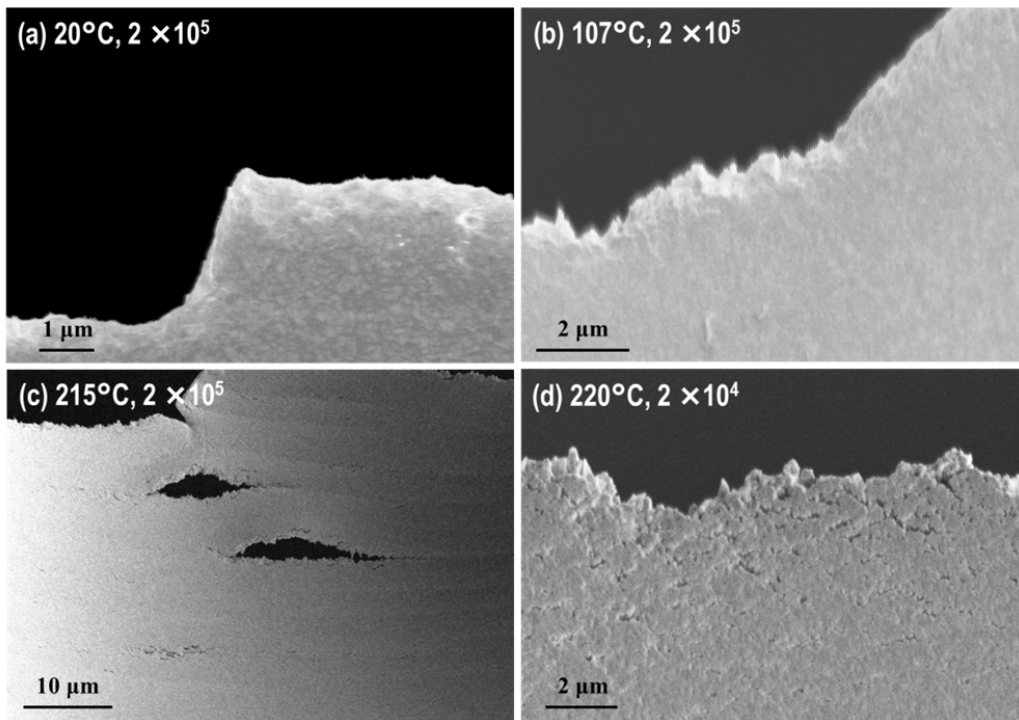


Figure 3. SEM micrographs of the failure morphology of 960 nm Au films tested at several different temperatures as marked in the images.

4. Discussions

The observations of a decreasing loading/unloading slope and flow stress with rising temperature is similar to the findings in a previous study on the mechanical behavior of Cu thin films at temperatures up to 430°C [27]. This behavior was attributed to diffusion-facilitated grain boundary sliding and dislocation climb. Another study on nano-crystalline Au films at temperatures up to 110°C [21] also reported grain boundary sliding as the dominant deformation mechanism with an increasing contribution of dislocation climb at higher temperatures.

While a comprehensive study with a broader range of strain rates at different temperatures would be required to calculate the activation volume and to precisely determine the dominant deformation mechanisms, the micrographs in Figure 3 suggest that gold films deform at elevated temperature via grain boundary-mediated mechanisms such as grain boundary sliding or diffusional creep, and the stress-strain curves are generally consistent with this notion.

The hysteresis loops observed in Figure 2 are consistent with grain boundary sliding: As grains slide past one another, back stresses build up at triple junctions that eventually stop the sliding. During unloading, these back stresses drive a recovery process that leads to a hysteresis loop and a reduced modulus [23, 34-36]. As the temperature increases, grain boundary sliding occurs more easily and the modulus decreases further. Reduced moduli have also been reported for room temperature experiments on Al and Au thin films, where the reduction was attributed to grain boundary sliding [28, 37, 38].

As the temperature rises, the rate of diffusion increases and diffusional creep becomes an important deformation mechanism in addition to dislocation plasticity, significantly lowering the flow stress of the film. Ashby et al. [39] have formulated a grain boundary diffusion model that includes grain boundary sliding attributes. According to this model, the strain rate is given by

$$\dot{\epsilon}_{gb} = \frac{330 \delta D_{0,gb} \Omega}{RT} \frac{1}{d^3} \left[\sigma - \frac{0.72 \Gamma}{d} \right] \exp \left[-\frac{Q_{gb}}{RT} \right] \quad (2)$$

where Q_{gb} (85 kJ/mol [40]) and $D_{0,gb}$ (6.2×10^{-7} m²/s [40]) are the activation energy and pre-exponential coefficient for the grain boundary diffusivity respectively, R is the ideal gas constant, T is the absolute temperature, δ is the width of the grain boundary (5×10^{-10} m [40, 41]), Ω is the molar volume (1.44×10^{-5} m³/mol [42]), d is the grain size, h the film thickness and Γ is the grain-boundary free energy (0.2 J/m² for nano-crystalline gold [41]). The values of the flow stress that correspond to the experimental strain rates are listed in Table II. Above 100°C, the theoretical flow stresses are smaller than the experimental values, indicating that grain boundary diffusion-mediated creep contributes to the deformation at these temperatures. Other models based on grain boundary diffusion such as Gibbs's model for creep in thin films [43] yield similar results. It should be noted, however, that models based on grain boundary diffusion predict flow stresses that are much lower than the experimental values at the highest temperatures. This observation suggests that there is a second deformation mechanism that operates in parallel and that requires a higher stress level. We suspect that this is a mechanism based on dislocation plasticity that ensures compatibility between regions of sliding grains. Wei et al. [44] developed a computational model that accounts for the coupling between grain boundary processes and dislocation plasticity that showed a transition at room temperature from dislocation plasticity to grain-boundary facilitated creep as the strain rate decreased. We expect that a similar model would provide a good description of the flow stress as a function of temperature.

The diffusion-facilitated grain boundary sliding mechanism is also consistent with the observation that the 960 nm film is much stronger than the 450 nm film (Table II), in contrast to the usual notion that smaller is stronger where thin films are concerned [9-11]. Within the

context of the Ashby model, this anomaly is readily explained as a grain size effect. The strain rate depends sensitively on the grain size, Eq. (2), and even the slightly larger grain sizes of the thicker film can result in significantly smaller strain rates (or yield stresses at the same strain rate). Moreover, creep as a result of surface/grain boundary diffusion as envisioned by Gibbs [43] will further lower the flow stress of the thinner films.

Our findings have direct implications for electronic devices or nano/micro structures that contain metal thin films. Most commercial finite element programs used to model these systems rely on Young's modulus, Poisson's ratio and yield strength to estimate stresses and strains in a structure. Our experiments show that anelastic effects induced by grain boundary sliding are important and that they can lead to a considerable lowering of the apparent stiffness. Moreover, diffusional creep can reduce the flow stress significantly at elevated temperatures and may lead to an unusual thickness dependence of the flow stress.

5. Summary

The mechanical behavior of thin sputter-deposited Au films has been studied at various temperatures and strain rates. Stress-strain curves at elevated temperature reveal a large decrease in yield strength and loading slope. We also observe an inverse size effect where the yield strength at elevated temperature decreases with decreasing temperature. This behavior is attributed to grain boundary mediated deformation processes such as grain boundary sliding.

6. Acknowledgments

The work presented in this paper was supported by the Air Force Office of Scientific Research under Grant FA9550-12-1-0098 (program manager Dr. Ali Sayir). The tensile samples were fabricated at the Center for Nanoscale Systems, a member of the National Nanotechnology Infrastructure Network, which is supported by the National Science Foundation under NSF Award ECS-0335765, and at the Harvard University Materials Research Science and Engineering Center, which is supported by the National Science Foundation under Award No. DMR-0820484. This work was also supported by the National Research Foundation of Korea (NRF) grant funded by the Korea government (MEST) (No. 2012R1A6A3A03037832).

7. References

- [1] J.S. Stolken, A.G. Evans, *Acta Mater*, 46 (1998) 5109-5115.
- [2] R.M. Keller, S.P. Baker, E. Arzt, *Acta Mater*, 47 (1999) 415-426.
- [3] M.A. Haque, M.T.A. Saif, *Acta Mater*, 51 (2003) 3053-3061.
- [4] R. Schwaiger, O. Kraft, *Acta Mater*, 51 (2003) 195-206.
- [5] H.D. Espinosa, B.C. Prorok, B. Peng, *J Mech Phys Solids*, 52 (2004) 667-689.
- [6] G.P. Zhang, C.A. Volkert, R. Schwaiger, P. Wellner, E. Arzt, O. Kraft, *Acta Mater*, 54 (2006) 3127-3139.
- [7] P.A. Gruber, J. Bohm, F. Onuseit, A. Wanner, R. Spolenak, E. Arzt, *Acta Mater*, 56 (2008) 2318-2335.
- [8] G.-D. Sim, Y.-S. Lee, S.-B. Lee, J.J. Vlassak, *Materials Science and Engineering: A*, 575 (2013) 86-93.
- [9] R.P. Vinci, J.J. Vlassak, *Annu Rev Mater Sci*, 26 (1996) 431-462.
- [10] W.D. Nix, *Metall Trans A*, 20 (1989) 2217-2245.
- [11] P.S. Alexopoulos, T.C. Osullivan, *Annu Rev Mater Sci*, 20 (1990) 391-420.
- [12] Y. Xiang, T. Li, Z.G. Suo, J.J. Vlassak, *Appl Phys Lett*, 87 (2005).
- [13] N.S. Lu, X. Wang, Z.G. Suo, J. Vlassak, *Appl Phys Lett*, 91 (2007) 221909.
- [14] G.D. Sim, S. Won, C.Y. Jin, I. Park, S.B. Lee, J.J. Vlassak, *J Appl Phys*, 109 (2011).
- [15] G.D. Sim, Y. Hwangbo, H.H. Kim, S.B. Lee, J.J. Vlassak, *Scripta Materialia*, 66 (2012) 915-918.
- [16] P.A. Gruber, S. Olliges, E. Arzt, R. Spolenak, *J Mater Res*, 23 (2008) 2406-2419.
- [17] S.P. Baker, A. Kretschmann, E. Arzt, *Acta Mater*, 49 (2001) 2145-2160.
- [18] D. Weiss, H. Gao, E. Arzt, *Acta Mater*, 49 (2001) 2395-2403.
- [19] M. Legros, K.J. Hemker, A. Gouldstone, S. Suresh, R.M. Keller-Flaig, E. Arzt, *Acta Mater*, 50 (2002) 3435-3452.
- [20] M.A. Haque, M.T.A. Saif, *Thin Solid Films*, 484 (2005) 364-368.
- [21] N.J. Karanjgaokar, C.S. Oh, J. Lambros, I. Chasiotis, *Acta Mater*, 60 (2012) 5352-5361.
- [22] H.B. Huang, F. Spaepen, *Acta Mater*, 48 (2000) 3261-3269.
- [23] D.Y.W. Yu, in: *Harvard University, United States -- Massachusetts*, 2003, pp. 163-163 p.
- [24] M. Zupan, M.J. Hayden, C.J. Boehlert, K.J. Hemker, *Exp Mech*, 41 (2001) 242-247.
- [25] M. Zupan, K.J. Hemker, *Mat Sci Eng a-Struct*, 319 (2001) 810-814.
- [26] M. Smolka, C. Motz, T. Detzel, W. Robl, T. Griesser, A. Wimmer, G. Dehm, *Rev Sci Instrum*, 83 (2012).
- [27] G.D. Sim, J.H. Park, M.D. Uchic, P.A. Shade, S.B. Lee, J.J. Vlassak, *Acta Mater*, (2013).
- [28] R.P. Vinci, G. Cornella, J.C. Bravman, *AIP Conference Proceedings*, 491 (1999) 240-248.
- [29] R.D. Emery, G.L. Povirk, *Acta Mater*, 51 (2003) 2079-2087.
- [30] R.D. Emery, G.L. Povirk, *Acta Mater*, 51 (2003) 2067-2078.
- [31] K. Jonnalagadda, N. Karanjgaokar, I. Chasiotis, J. Chee, D. Peroulis, *Acta Mater*, 58 (2010) 4674-4684.
- [32] Z.H. Jiang, X.L. Liu, G.Y. Li, Q. Jiang, J.S. Lian, *Appl Phys Lett*, 88 (2006).
- [33] R. Schwaiger, B. Moser, M. Dao, N. Chollacoop, S. Suresh, *Acta Mater*, 51 (2003) 5159-5172.
- [34] C. Zener, *Phys Rev*, 60 (1941) 906-908.
- [35] T.S. Ke, *Phys Rev*, 71 (1947) 533-546.
- [36] R. Raj, M.F. Ashby, *Metall Trans*, 2 (1971) 1113-&.
- [37] A.J. Kalkman, A.H. Verbruggen, G.C.A.M. Janssen, *Appl Phys Lett*, 78 (2001) 2673-2675.
- [38] S.P. Baker, R.P. Vinci, T. Arias, *Mrs Bull*, 27 (2002) 26-29.
- [39] M.F. Ashby, R.A. Verrall, *Acta Metall Mater*, 21 (1973) 149-163.
- [40] D. Gupta, *J Appl Phys*, 44 (1973) 4455-4458.
- [41] S. Sakai, H. Tanimoto, E. Kita, H. Mizubayashi, *Phys Rev B*, 66 (2002).
- [42] C.J. Smithells, W.F. Gale, T.C. Totemeier, *Smithells metals reference book*, 8th ed., Elsevier Butterworth-Heinemann, Amsterdam ; Boston, 2004.
- [43] G.B. Gibbs, *Philos Mag*, 13 (1966) 589-&.
- [44] Y.J. Wei, A.F. Bower, H.J. Gao, *Acta Mater*, 56 (2008) 1741-1752.